

AetheRock: An Arm-Worn Robot Teaching System for Force-Guided Vision-Tactile Learning

Hong Li¹, Yue Xu¹, Yihan Tang¹, Yankang Dong¹, Chenyuan Liu¹, Chenyang Yu¹,
 Xuyang Li^{1,*}, Siyuan Huang⁴, Yujun Shen², Nan Xue², Yong-Lu Li^{1,3†}
¹Shanghai Jiao Tong University, ²Ant Group, ³Shanghai Innovation Institute
⁴Beijing Institute for General Artificial Intelligence (BIGAI),
 {hong_li, yonglu.li}@sjtu.edu.cn

Abstract: Force and tactile sensing are indispensable in contact-rich manipulation. However, force-aware robot learning faces critical challenges due to the incompatible assembly of tactile and force sensors in handheld or wearable devices. To address these limitations, we first introduce **AetheRock** for gripper-force, vision, and tactile data collection, which is an arm-worn device featuring a modular and easily manufactured visuo-tactile sensor, **GelSlim-MiniFab**, at the fingertip, a resistive pressure sensor at the human finger contact region, a customized PCB module, and a wearable kit for comfortable and robust collection. Building on this, we propose **ForceVT**, a representation learning framework that uses force and vision to guide fidelity-agnostic tactile learning, enabling robust inference in *any tactile situation*. Real-world experiments show that AetheRock achieves qualified data efficiency and that ForceVT effectively alleviates inefficiencies when visuo-tactile sensors exhibit manufacturing and utilization inconsistencies. Overall, our work mitigates the limitations of gripper-force vision-tactile robot learning through innovative hardware design and algorithms.

Project page: <https://rhos.ai/research/AetheRock>.

Keywords: Force-Tactile Sensor, Robot System, Contact-rich Manipulation

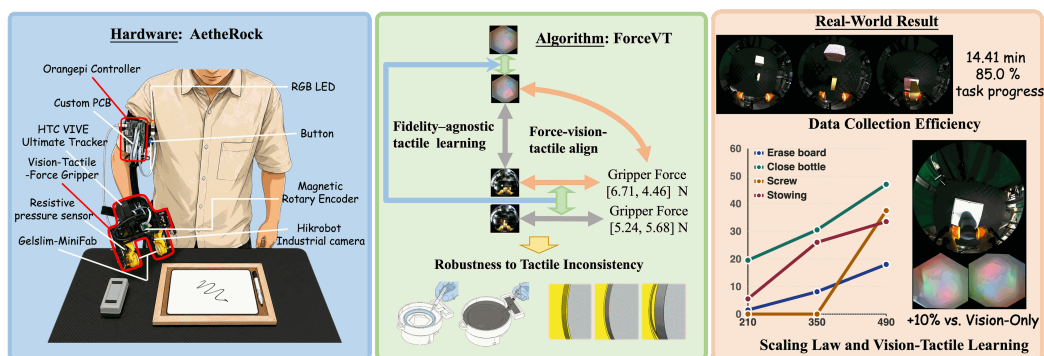


Figure 1: We present a hardware and algorithm co-design robot teaching system. We introduce AetheRock (Left), an arm-worn device for collecting gripper force, vision, and tactile data. We further develop the ForceVT algorithm (Middle) to improve robust tactile utilization. We evaluate the effectiveness of the hardware and algorithm in real-world robotics (Right).

*This work was done during an internship at Shanghai Jiao Tong University.

†Correspondence to: Yong-Lu Li <yonglu.li@sjtu.edu.cn>.

1 Introduction

Recent advances in robot learning have driven substantial progress in imitation learning [1, 2] and vision-language-action (VLA) [3, 4, 5, 6] models. These are driven by large-scale robot manipulation data. While teleoperation yields the highest benefit in robot learning, it is labor-intensive and scene-limited. To reduce the complexity of data acquisition, many works involve egocentric human demonstrations [7, 8, 9] and UMI [10, 11] data. Human demonstrations are cheaper and more massive, but exhibit low adaptability to robot embodiments. UMI, with the same end effector and relative trajectory movement as a real robot, shows huge potential for collecting robot teaching data.

To address contact-rich manipulation, current research has developed the vision-tactile UMI [12, 13] structure device. However, for necessary force sensing, few works [14, 15] use a *high-cost* force sensor between the gripper and a rear handle. Contact-rich manipulation is directly related to gripper force and tactile feedback. Applying a 6-axis F/T sensor in existing works faces challenges, such as a large size that is difficult to adapt to a robot gripper, and high costs that hinder mass production. Visuo-tactile sensors are widely applied in contact-rich tasks due to their easy-to-manufacture and complete contact information. However, manufacturing usually produces slight differences due to imperfect gel mixing. Furthermore, utilization will slowly change the fidelity and sensitivity, caused by the edge gel lifting or being hit. These inconsistencies cannot be thoroughly eliminated, which also influences the model’s performance. Currently, since the tactile sensor cost is relatively high, transferring to a new sensor due to slight scratches or lifted silicone would be a waste of resources.

To address uponn challenges, we firstly present **AetheRock**, as shown in the left of Figure 1, an arm-worn robot teaching system designed for force, vision and tactile data collection. Utilizing finger operations similar to FreeTacMan [16], the system collects UMI end-effector data enhanced by multi-sensor perception. Our system introduces **three key innovations**: (1) A resistive pressure sensor adapted to the central controller for robust gripper force collection; (2) A new visuo-tactile **GelSlim-MiniFab** builds on the optics and PCB design of GelSlim 4.0 [17], with low-cost manufacturing and easy-to-repair features; (3) Modular PCBs combined with an arm-worn kit for stable connectivity and comfortable collection. With AetheRock, users can collect force and tactile data for robot learning over a continuous window four times longer than UMI’s, with 100% data usability.

Building on the proposed AetheRock robot data collection system, we propose **ForceVT**, a force-guided vision-tactile learning algorithm, as shown in the middle of Figure 1. To reduce the influence of vision-tactile inconsistency during manufacturing and deployment, we design multi-fidelity tactile sensors, including high-fidelity sensors with perfect tactile signals and low-fidelity sensors with different degrees of damage, and use vision and force to guide fidelity-agnostic tactile learning. Finally, as shown on the right of Figure 1, we evaluate data collection efficiency on six robotic tasks and evaluate post-training scaling laws and vision-tactile learning on four robotic tasks. Experiments demonstrate that our hardware provides qualified data quality and that incorporating force-tactile information with the proposed algorithm improves policy performance and robustness.

In summary, our primary contributions include: (1) An arm-worn robot teaching system, AetheRock, to robustly and conformably collect gripper force, vision, and tactile robot data. (2) A multi-sensor assembly design, including the new visuo-tactile sensor GelSlim-MiniFab with low-cost manufacturing and easy-to-repair features, and a resistive pressure sensor for gripper force collection. (3) A force-guided vision-tactile learning algorithm, ForceVT, uses force and vision to guide fidelity-agnostic tactile representation learning, enabling robustness in any tactile situation.

2 Related Work

Robot Data Collection System. Universal Manipulation Interface(UMI) shares the same end-effector as the real robot and learns using the relative movement of the executor, which exhibits great potential for general robot manipulation models. FastUMI [18] improves the SLAM system with RealSense T265. RoboPocket [19] integrates its system within an iPhone. exUMI [12], Free-TacMan [16], TouchGuide [20], TacUMI [14] incorporate visuo-tactile sensors. ForceMimic [21]

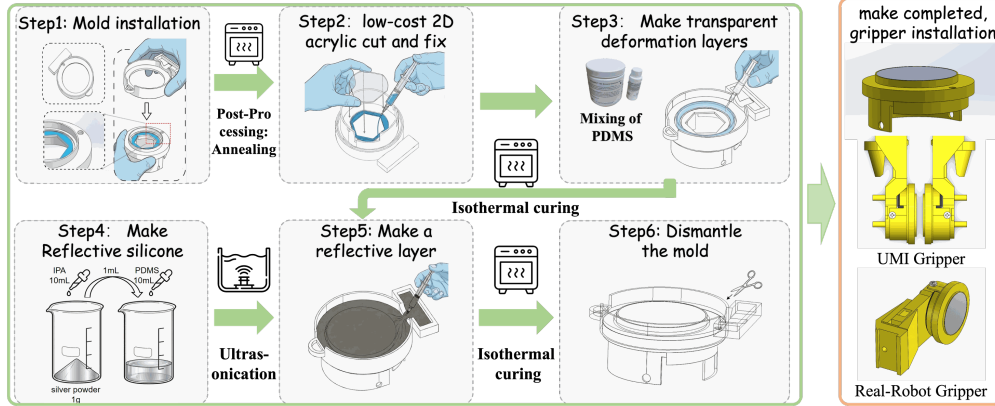


Figure 2: Manufacturing of GelSlim-MiniFab. Inspired by the GelSlim 4.0 [17] optics and PCB design, we propose GelSlim-MiniFab, including low-cost manufacturing, easy reparability, and adaptability to multiple gripper features.

and OmniUMI [15] integrate 6-axis F/T sensors. Although existing works integrate more sensors, gripper force is not considered in current works, which is significant for contact-rich tasks. We propose an Arm-Worn Robot Teaching System, AetheRock, to collect force, vision and tactile data.

Visuo-Tactile Sensor Design. Various tactile sensors are designed for contact-rich manipulation, including visuo-tactile [22, 23, 24], capacitive [25, 26, 27], resistive [28, 29], etc. Visuo-tactile sensors are widely applied, offering ease of fabrication and low cost. However, all tactile sensors have a limited lifecycle, and their gel are easily destroyed. GelSlim 4.0 [17] is an open-source tactile sensor. Although it provides complete manufacturing details, the dependent devices are high-cost, and the repair process is tedious. To address these challenges and provide a hardware base for algorithms resolving manufacturing and utilization inconsistencies, we propose GelSlim-MiniFab.

Vision-Tactile Learning. Vision-tactile learning focuses on training a tactile encoder by aligning tactile features with vision features or injecting tactile tokens into vision features. More closely related to robot action models, many works aim to incorporate tactile tokens into VLA models. VTLA [30] trains a Vision-Tactile-Language-Action model by integrating vision and tactile inputs through cross-modal language grounding. OmniVTLA [31] utilizes a dual-path tactile framework for the encoder and semantically aligned algorithms between language and vision. TacVLA [32] and AT-VLA [33] employ a gating mechanism to achieve adaptive multimodal fusion. Tactile-VLA [34] divides the model’s intentions into precise physical actions and a reasoning module to obtain vision-tactile perceptions. HapticVLA [35] studies training with offline data involving haptics and deployment without direct haptic feedback during inference. TacFiLM [36] extends FiLM [37] fusion to vision-tactile learning. Overall, these works rely on ideal tactile sensors, overlooking visuo-tactile inconsistencies caused by manufacturing and utilization. Therefore, we propose an algorithm to study the robust utilization of tactile sensors.

3 AetheRock Data Collection System

3.1 Gelslim-MiniFab

Inspired by GelSlim 4.0 [17] optics and PCB design, we propose **GelSlim-MiniFab**, as shown in Figure 2, which is a visuo-tactile sensor with low-cost manufacturing and easy-to-repair features. GelSlim-MiniFab has three key innovations: (1) Low optical requirements, which permit users to use 2D-cut acrylic rather than high-cost 3D acrylic. (2) Replaceable RGB plates and silicone cases, which permit us to quickly repair damaged RGB and silicone cases. (3) Easy assembly onto robot grippers and UMI devices. Detailed manufacturing and visualize refer to supplementary material.

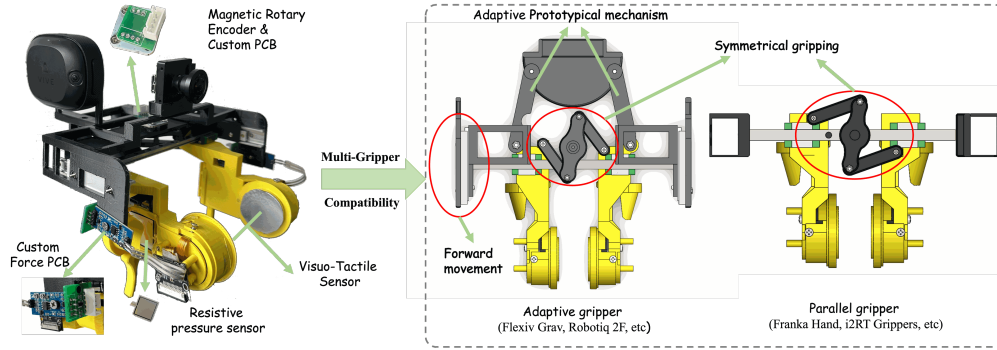


Figure 3: AetheRock hardware system. An arm-worn data collection system for force, vision, and tactile data collection, which includes two general grippers, an adaptive gripper and a parallel gripper, can be easily adapted to other robot grippers.

3.2 Hardware Design

Multi-sensor Data Collection Module. As shown in Figure 3, for visual sensing, we follow RDT2 [38] and use a Hikrobot MV-CB060-10UM/UC industrial camera with an exposure of 20,000. For motion tracking, we adopt an HTC VIVE Ultimate Tracker and adapt it to a headless setup following DexCap [39]. Following exUMI [12], gripper width is estimated using a low-cost AS5600 magnetic rotary encoder with an improved PCB design for compactness and robustness. To improve the generalizability of AetheRock, we develop both parallel and adaptive gripper designs, which can generalize to other grippers. To avoid the size and cost limitations of 6-axis F/T sensors, we use a low-cost resistive pressure sensor mounted at human finger contact regions for force collection.

Custom PCB and Wearable Kit for Comfort and Robust Collection. System robustness is essential for continuous data collection and compact hardware. We design three PCBs for connectivity: one at the central Orange Pi controller to interface with other modules, one at the magnetic rotary encoder for compactness and robust connection, and one at the resistive pressure sensor integrated with an ADC module and connected to the OrangePi via I2C. Additionally, we incorporate a magnetic suction armband and an optional wristband for ergonomic design, allowing the arm and wrist to share most of AetheRock’s weight and enabling data collection for over two hours.

3.3 Data Process

System Time Calibration. To guarantee precise temporal alignment across the PC and OrangePi central control during data collection, we developed a localized high-precision Network Time Protocol (NTP) synchronization mechanism. The PC acts as the primary time server, while the OrangePi controller functions as a dedicated client. By enforcing high-frequency local polling for frequent synchronization and isolating it from external public time pools, we achieve highly stable temporal alignment across all sensor streams with an average synchronization latency of 10 ms.

Tactile Calibration. To ensure spatial consistency and eliminate perspective distortion in the tactile observations, we develop a geometric calibration pipeline. First, the gel region is isolated from the surrounding support frame using adaptive thresholding and polygonal approximation. Next, we reconstruct the complete sensor geometry by extrapolating the valid contour edges to recover the hidden vertices, effectively capturing the inherent perspective tilt and spatial asymmetry. Finally, a homography transformation maps these distorted physical vertices onto a dynamically calculated, mathematically ideal regular polygon centered within the image frame. This spatial warping process yields a standardized tactile vision, eliminating geometric inconsistencies across hardware devices.

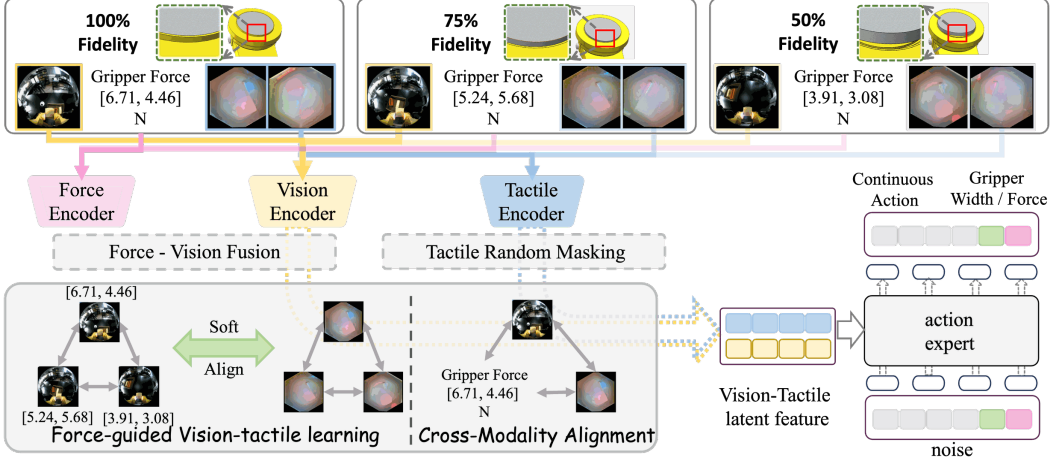


Figure 4: Schematic framework of the proposed ForceVT. Multi-fidelity tactile data are augmented via random masking, followed by modality-specific encoding. The force-guided vision-tactile learning module leverages fused vision-force features to guide tactile representation learning. Finally, the cross-modality alignment module computes cosine similarities across all modalities, while the conditioned vision-tactile features generate continuous actions.

Resistive Pressure Sensor Calibration. To process the resistive pressure sensor readings, we implement a piecewise linear calibration protocol via a 16-bit I2C ADC interface. The raw analog signals are first mapped to the system voltage domain. To mitigate sensor noise and hardware saturation, we apply a thresholding mechanism: voltages below an effective threshold of 500 mV are zeroed, while the active response range (500–5000 mV) is linearly mapped to the target physical force span (50–1000 g). The final measurements are converted to standard Newtons (N).

4 Methodology

Based on our proposed visuo-tactile sensor, GelSlim-MiniFab, we fabricate sensors across various fidelities to collect aligned wrist vision, tactile and gripper force data. Furthermore, we propose a force-guided vision-tactile learning algorithm to learn fidelity-agnostic tactile representations, ensuring robustness in any tactile situation. Figure 4 presents ForceVT, a post-training framework featuring Robust Tactile Representation Learning for robustness to tactile variations and Cross-Modality Soft Alignment for preserving consistency between the relational structure of tactile features and that of fused vision–force features.

4.1 Robust Tactile Representation Learning

To increase tactile diversity and improve robustness to any tactile situation, we introduce Tactile Random Masking, which perturbs tactile observations through stochastic spatial masking. Following DINOv3 [40], for each training batch, a ratio $\rho \in (0, 1)$ of tactile samples is randomly selected for masking, where a fraction $\eta \in (0, 1)$ of spatial patches in each selected sample is randomly replaced. For tactile observations from the k -th fidelity sensor, the process is formulated as:

$$\tilde{T}^{(k)} = \mathcal{M}_{\rho, \eta}(T^{(k)}), \quad (1)$$

where $\mathcal{M}_{\rho, \eta}$ denotes the masking operator, and $T^{(k)}$ and $\tilde{T}^{(k)}$ represent the raw and masked tactile observations from the k -th fidelity sensor, respectively.

The masked tactile input $\tilde{T}^{(k)}$, together with aligned wrist vision I_v and force data F , is encoded by modality-specific encoders to obtain latent representations:

$$z_v = E_v(I_v), \quad z_f = E_f(F), \quad \tilde{z}_t^{(k)} = E_t(\tilde{T}^{(k)}), \quad (2)$$

where E_v , E_f , and E_t denote the vision, force, and tactile encoders, respectively.

4.2 ForceVT: Force Guided Vision Tactile Learning

We first fuse vision and force features with a lightweight fusion module:

$$z_{vf} = \mathcal{F}(z_v, z_f), \quad (3)$$

where z_{vf} denotes the fused vision-force representation.

To learn fidelity-agnostic tactile representations, we introduce a soft alignment that transfers relational similarity across different tactile fidelities from the fused vision force space to tactile space:

$$\mathcal{L}_{\text{soft}} = \frac{1}{N^2} \sum_{i,j} \left\| \text{sim}(z_{vf}^i, z_{vf}^j) - \text{sim}(\tilde{z}_t^{i,(k_i)}, \tilde{z}_t^{j,(k_j)}) \right\|_2^2, \quad (4)$$

where k_i and k_j denote the tactile fidelity levels of samples i and j , respectively. Thus, the tactile similarity is computed between tactile representations that may come from different fidelity sensors.

To achieve cross-modality alignment, we adopt a contrastive loss between vision force and tactile representations:

$$\mathcal{L}_{\text{con}} = -\frac{1}{N} \sum_{i=1}^N \log \frac{\exp(\text{sim}(z_{vf}^i, \tilde{z}_t^{i,(k_i)})/\tau)}{\sum_{j=1}^N \exp(\text{sim}(z_{vf}^i, \tilde{z}_t^{j,(k_j)})/\tau)}, \quad (5)$$

where $\text{sim}(\cdot, \cdot)$ denotes cosine similarity, τ is a temperature parameter, and N is the batch size.

During inference, the policy predicts continuous actions a , including end-effector relative pose, gripper width, and force, from vision and tactile features. The action objective is defined as:

$$\mathcal{L}_{\text{act}} = \mathcal{L}_{\text{expert}}(\pi_{\text{expert}}(z_v \oplus z_t), a), \quad (6)$$

where $\mathcal{L}_{\text{expert}}$ denotes the expert action loss. In summary, the overall objective is:

$$\mathcal{L} = \lambda_1 \mathcal{L}_{\text{soft}} + \lambda_2 \mathcal{L}_{\text{con}} + \lambda_3 \mathcal{L}_{\text{act}}, \quad (7)$$

where λ_1 , λ_2 , and λ_3 are adjustable weighting parameters.

5 Experiment

5.1 Experiment Setup



Figure 5: Real-world rollout of the data efficiency policy. Only fisheye camera input to the model.

Task	Data Collection		Task progress
	Number of demos	Duration (min)	
Clamp Seal	229	28.86	60.0%
Towel Hanging	206	27.60	47.5%
Pick Bread	199	17.16	64.5%
Erase Board	215	26.16	26.0%
Pick Block	214	14.41	85.0%
Insert Flower	212	24.72	22.0%

Table 1: Data collection efficiency and policy performance on vision-only tasks.

Tasks and Data Collection. In our experiments, we included tasks ranging from simple pick-and-place to long-horizon. We initially collected about 200 episodes across six tasks. Each demonstration collection involved single-direction generation. Subsequently, we selected four tasks and employed three levels of tactile fidelity to simulate inconsistency. We divided the data into groups of 70 episodes each, collecting five groups at 100% fidelity, and one group at 75% and 50% fidelity.

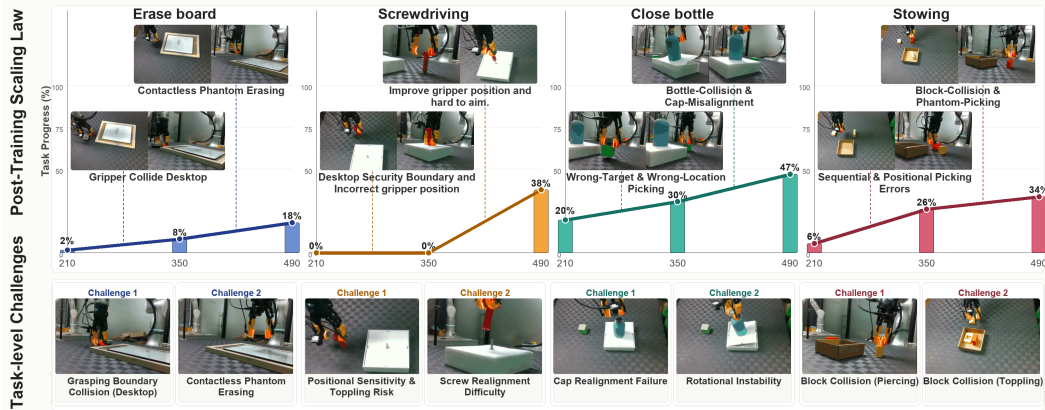


Figure 6: Post-training scaling law across four tasks. The bottom section details the challenges for each task, and the midpoint of the line indicates the inflection point as data is added.

Evaluation Methods. We first evaluated data collection efficiency across six tasks with single-direction generation. We then used subsets of three, five, and all seven groups of data to assess post-training scaling laws. Finally, we validated ForceVT and the baselines using all data. We included the following baselines: a) VisTacLinear: this method fuses vision and tactile features using simple linear fusion. b) TacFiLM [36]: this method integrates tactile tokens into the vision encoder via FiLM [37]. c) TactileConcat: as described in TacFiLM, we implemented the tactile concatenation strategy used in prior works [41, 42, 34, 43, 44, 45], where the tactile encoder was T3 [46].

Training and Inference. Our experiments were implemented on $\pi_{0.5}$ [4], revised to learn the relative pose as in UMI [10]. All trained models performed inference on a Flexiv Rizon 4 robot arm with a Flexiv Grav adaptive gripper. For each model, we ran inference 20 times and computed the mean task progress following $\pi_{0.5}$ [4], which reflects fine-grained task progress. For the single-direction setting, the objects maintained a consistent relative pose and were adjusted only along the vertical direction. For the global generalist setting, we moved the objects to five random positions and performed inference four times at each position. The detailed training and inference settings, as well as the task progress definition, are provided in the supplementary material.

5.2 Experimental Results

Data Collection Efficiency. Figure 5 and Table 1 show the results of data collection efficiency across six tasks. Overall, without involving global generalization, pick-and-place tasks can attain over an 80% task progress for rigid objects and a 60% task progress for soft objects with less than 20 minutes of demonstrations. Complex actions, such as handling and erasing, can achieve a certain level of performance with 30 minutes of demonstrations, but limited perception hampers success, for instance, hitting the desktop or performing contactless phantom erasing in the erase board task. The clamp seal task requires rigid gripper width control, and the 60% task progress demonstrates robust data quality. The insert flower task requires reasoning about the gripper pose, erroneous positions obstruct the observation, which is difficult for the current model.

Post-training Scaling Law. Figure 6 shows the results of the post-training scaling law. Overall, with data scaling, the policy performance improves to a certain extent. When extending data collection and inference to a global generalization setting, the policy performance declines significantly compared to Table 5. Limited data generally results in weak perception. For instance, the policy knocks over the screw socket when trained with 210 to 350 episodes of data. Furthermore, relying solely on the wrist fisheye camera makes alignment actions difficult. For example, the close bottle and screwdriving tasks face challenges in aligning the lid with the cup and the socket with the screw. Additionally, some failures occur due to reducing the gripper width too early or loosening the grip-

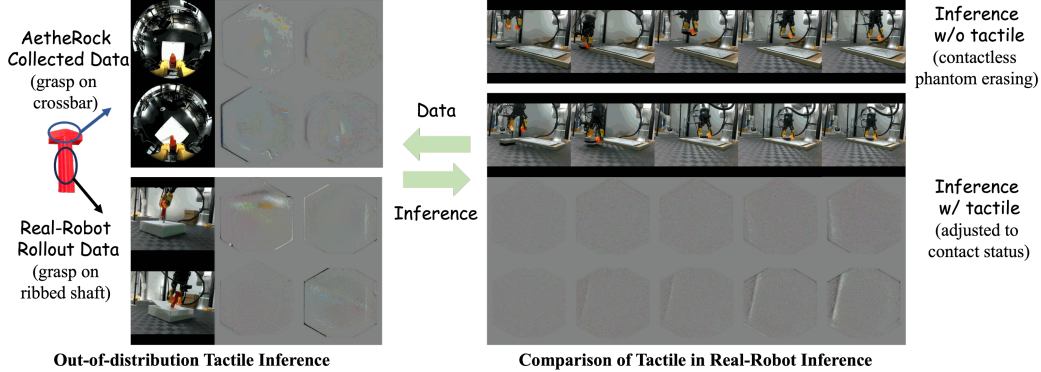


Figure 7: Visualization of tactile challenges in training and inference. The left shows grasp pose out-of-distribution during training. The right shows inference with or without tactile sensing.

per during movement. Specifically, two-thirds of the failures in the stowing task fall into these two categories, while the remaining failures involve collisions with the block.

Methods	Erase Board	Screwdriving	Close Bottle	Stowing
Vision-only	18.0%	38.0%	47.0%	34.0%
VisTacLinear	31.5%	31.0%	50.5%	45.5%
TacFiLM [36]	5.5%	36.5%	39.0%	43.5%
TactileConcat [46]	20.0%	9.0%	22.5%	30.0%
ForceVT (Ours)	49.0%	48.5%	58.0%	55.0%

Table 2: Real-world evaluation of the vision-tactile policy across contact-rich tasks.

Tactile Fidelity	100%	75%	50%	Avg.
VisTacLinear	50.5%	30.5%	26.5%	35.8%
TacFiLM [36]	39.0%	18.5%	14.5%	24.0%
TactileConcat [46]	22.5%	15.5%	18.0%	18.7%
ForceVT (Ours)	58.0%	57.0%	53.0%	56.0%

Table 3: Policy robustness on the bottle-closing across different tactile fidelities.

Vision-Tactile Learning. Tables 2 and 3 report vision tactile policy performance and robustness, respectively. Overall, tactile sensing improves policy performance in both VisTacLinear and ForceVT. Tactile signals provide status guidance for policy progression. As shown in the inference part of Figure 7, policies with tactile sensing tend to move toward contact signals, whereas policies without tactile sensing exhibit contactless phantom actions. An exception is screwdriving, where the primary challenge arises from out-of-distribution (OOD) of inference tactile, as illustrated in the data part of Figure 7. This issue is caused by inconsistent grasp positions, where grasping occurs on a crossbar during training but on a ribbed shaft during inference. TacFiLM and TactileConcat generally perform worse than simple linear fusion, indicating that fusing vision and tactile modalities too early is less effective than later latent fusion and exhibits weaker generalization across tactile sensors, as our sensor is not trained on the T3 model. From Table 3, baseline methods exhibit substantial performance degradation when tactile fidelity decreases, with a maximum decrease close to 20%, whereas our method remains robust with changes below 5%. This demonstrates the robustness of our method across different tactile situations.

6 Conclusion

In this paper, we focus on hardware-algorithm co-design to propose a robotic teaching system. First, we present AetheRock, an arm-worn device for collecting gripper force, vision, and tactile data. Next, we propose ForceVT to learn robust vision-tactile representations through force guidance. We validate the data collection efficiency of AetheRock, the post-training scaling laws, and the vision-tactile learning algorithm on real-world robotic tasks. In summary, AetheRock collects robust multi-sensor data, and our algorithm improves visuo-tactile robustness.

7 Limitations

A primary limitation of this work is an inconsistency in tactile contact signals between training and inference. AetheRock enables flexible manipulation and data collection, but real-robot inference, with its limited perception and execution, produces edge contacts and pad contacts. Developing algorithms and involving inference feedback in data collection to solve this generalization issue will be a focus of future work. Additionally, tactile sensing provides contact texture signals and also includes shear force perception. Assembling a robot system with a low-cost 6-axis F/T sensor, Coin-FT [47], can better align with tactile signals. Finally, tactile sensors show improvement in our work with contact status guidance signals, but this is weak due to our current study concentrating on post-training. Studying pre-training with a large amount of data will be future work.

References

- [1] C. Chi, Z. Xu, S. Feng, E. Cousineau, Y. Du, B. Burchfiel, R. Tedrake, and S. Song. Diffusion policy: Visuomotor policy learning via action diffusion. *The International Journal of Robotics Research*, 44(10-11):1684–1704, 2025.
- [2] T. Z. Zhao, V. Kumar, S. Levine, and C. Finn. Learning fine-grained bimanual manipulation with low-cost hardware. *arXiv preprint arXiv:2304.13705*, 2023.
- [3] K. Black, N. Brown, D. Driess, A. Esmail, M. Equi, C. Finn, N. Fusai, L. Groom, K. Hausman, B. Ichter, et al. *pi_0*: A vision-language-action flow model for general robot control. *arXiv preprint arXiv:2410.24164*, 2024.
- [4] P. Intelligence, K. Black, N. Brown, J. Darpinian, K. Dhabalia, D. Driess, A. Esmail, M. Equi, C. Finn, N. Fusai, et al. $\pi_{0.5}$: a vision-language-action model with open-world generalization. *arXiv preprint arXiv:2504.16054*, 2025.
- [5] S. Liu, L. Wu, B. Li, H. Tan, H. Chen, Z. Wang, K. Xu, H. Su, and J. Zhu. Rdt-1b: a diffusion foundation model for bimanual manipulation. In *International Conference on Learning Representations*, volume 2025, pages 29982–30009, 2025.
- [6] M. J. Kim, K. Pertsch, S. Karamcheti, T. Xiao, A. Balakrishna, S. Nair, R. Rafailov, E. Foster, G. Lam, P. Sanketi, et al. Openvla: An open-source vision-language-action model. *arXiv preprint arXiv:2406.09246*, 2024.
- [7] R. Punamiya, S. Kareer, Z. Liu, J. Citron, R.-Z. Qiu, X. Cai, A. Gavryushin, J. Chen, D. Li-conti, L. Y. Zhu, et al. Egoverse: An egocentric human dataset for robot learning from around the world. *arXiv preprint arXiv:2604.07607*, 2026.
- [8] A. S. Chen, S. Nair, and C. Finn. Learning generalizable robotic reward functions from” in-the-wild” human videos. *arXiv preprint arXiv:2103.16817*, 2021.
- [9] S. Gao, W. Liang, K. Zheng, A. Malik, S. Ye, S. Yu, W.-C. Tseng, Y. Dong, K. Mo, C.-H. Lin, et al. Dreamdojo: A generalist robot world model from large-scale human videos. *arXiv preprint arXiv:2602.06949*, 2026.
- [10] C. Chi, Z. Xu, C. Pan, E. Cousineau, B. Burchfiel, S. Feng, R. Tedrake, and S. Song. Universal manipulation interface: In-the-wild robot teaching without in-the-wild robots. *arXiv preprint arXiv:2402.10329*, 2024.
- [11] H. Choi, Y. Hou, C. Pan, S. Hong, A. Patel, X. Xu, M. R. Cutkosky, and S. Song. In-the-wild compliant manipulation with umi-ft. *arXiv preprint arXiv:2601.09988*, 2026.
- [12] Y. Xu, L. Wei, P. An, Q. Zhang, and Y.-L. Li. exumi: Extensible robot teaching system with action-aware task-agnostic tactile representation. *arXiv preprint arXiv:2509.14688*, 2025.
- [13] X. Zhu, B. Huang, and Y. Li. Touch in the wild: Learning fine-grained manipulation with a portable visuo-tactile gripper. *Advances in Neural Information Processing Systems*, 38: 153783–153812, 2026.
- [14] T. Cheng, K. Chen, L. Chen, L. Zhang, Y. Zhang, Y. Ling, M. Hamad, Z. Bing, F. Wu, K. Sharma, et al. Tacumi: A multi-modal universal manipulation interface for contact-rich tasks. *arXiv preprint arXiv:2601.14550*, 2026.
- [15] S. Luo, Y. Li, Y. Hu, C. Yu, C. Xu, J. Zhang, G. Yao, T. Huang, R. He, and Z. Wang. Omniumi: Towards physically grounded robot learning via human-aligned multimodal interaction. *arXiv preprint arXiv:2604.10647*, 2026.
- [16] L. Wu, C. Yu, J. Ren, L. Chen, Y. Jiang, R. Huang, G. Gu, and H. Li. Freetacman: Robot-free visuo-tactile data collection system for contact-rich manipulation. *arXiv preprint arXiv:2506.01941*, 2025.

- [17] A. Sipos, W. v. d. Bogert, and N. Fazeli. Gelslim 4.0: Focusing on touch and reproducibility. *arXiv preprint arXiv:2409.19770*, 2024.
- [18] Z. Zhaxizhuoma, K. Liu, C. Guan, Z. Jia, Z. Wu, X. Liu, T. Wang, S. Liang, P. Chen, P. Zhang, et al. Fastumi: A scalable and hardware-independent universal manipulation interface with dataset. In *Conference on Robot Learning*, pages 3069–3093. PMLR, 2025.
- [19] J. Fang, W. Chen, H. Xue, F. Zhou, T. Le, Y. Wang, Y. Zhang, J. Lv, C. Wen, and C. Lu. Robopocket: Improve robot policies instantly with your phone. *arXiv preprint arXiv:2603.05504*, 2026.
- [20] Z. Zhang, J. Ma, X. Yang, X. Wen, Y. Zhang, B. Li, Y. Qin, J. Liu, C. Zhao, L. Kang, et al. Touchguide: Inference-time steering of visuomotor policies via touch guidance. *arXiv preprint arXiv:2601.20239*, 2026.
- [21] W. Liu, J. Wang, Y. Wang, W. Wang, and C. Lu. Forcecemic: Force-centric imitation learning with force-motion capture system for contact-rich manipulation. In *2025 IEEE International Conference on Robotics and Automation (ICRA)*, pages 1105–1112. IEEE, 2025.
- [22] C. Lin, H. Zhang, J. Xu, L. Wu, and H. Xu. 9dtact: A compact vision-based tactile sensor for accurate 3d shape reconstruction and generalizable 6d force estimation. *IEEE Robotics and Automation Letters*, 9(2):923–930, 2023.
- [23] M. Lambeta, P.-W. Chou, S. Tian, B. Yang, B. Maloon, V. R. Most, D. Stroud, R. Santos, A. Byagowi, G. Kammerer, et al. Digit: A novel design for a low-cost compact high-resolution tactile sensor with application to in-hand manipulation. *IEEE Robotics and Automation Letters*, 5(3):3838–3845, 2020.
- [24] W. Yuan, S. Dong, and E. H. Adelson. Gelsight: High-resolution robot tactile sensors for estimating geometry and force. *Sensors*, 17(12):2762, 2017.
- [25] O. Glauser, D. Panozzo, O. Hilliges, and O. Sorkine-Hornung. Deformation capture via soft and stretchable sensor arrays. *ACM Transactions on Graphics (TOG)*, 38(2):1–16, 2019.
- [26] T.-Y. Wu, L. Tan, Y. Zhang, T. Seyed, and X.-D. Yang. Capacitivo: Contact-based object recognition on interactive fabrics using capacitive sensing. In *Proceedings of the 33rd annual acm symposium on user interface software and technology*, pages 649–661, 2020.
- [27] B. Xu, L. Zhong, G. Zhang, X. Liang, D. Virtue, R. Madan, and T. Bhattacharjee. Cushsense: Soft, stretchable, and comfortable tactile-sensing skin for physical human-robot interaction. In *2024 IEEE International Conference on Robotics and Automation (ICRA)*, pages 5694–5701. IEEE, 2024.
- [28] S. Sundaram, P. Kellnhofer, Y. Li, J.-Y. Zhu, A. Torralba, and W. Matusik. Learning the signatures of the human grasp using a scalable tactile glove. *Nature*, 569(7758):698–702, 2019.
- [29] S. Stassi, V. Cauda, G. Canavese, and C. F. Pirri. Flexible tactile sensing based on piezoresistive composites: A review. *Sensors*, 14(3):5296–5332, 2014.
- [30] C. Zhang, P. Hao, X. Cao, X. Hao, S. Cui, and S. Wang. Vtla: Vision-tactile-language-action model with preference learning for insertion manipulation. *Biomimetic Intelligence and Robotics*, page 100333, 2026.
- [31] Z. Cheng, Y. Zhang, W. Zhang, H. Li, K. Wang, L. Song, and H. Zhang. Omnivtla: Vision-tactile-language-action model with semantic-aligned tactile sensing. *arXiv preprint arXiv:2508.08706*, 2025.

- [32] K. Zhang, H. Zhang, Z. Xu, Z. Zhang, M. R. I. Prince, X. Li, X. Han, Y. Zhou, A. Ajoudani, and Y. She. Tacvla: Contact-aware tactile fusion for robust vision-language-action manipulation. *arXiv preprint arXiv:2603.12665*, 2026.
- [33] X. Li, M. Cai, J. Xu, J. Zhu, H. Fan, Y. Shen, G. Ren, and H. Dong. At-vla: Adaptive tactile injection for enhanced feedback reaction in vision-language-action models. *arXiv preprint arXiv:2605.07308*, 2026.
- [34] J. Huang, S. Wang, F. Lin, Y. Hu, C. Wen, and Y. Gao. Tactile-vla: unlocking vision-language-action model’s physical knowledge for tactile generalization. *arXiv preprint arXiv:2507.09160*, 2025.
- [35] K. Gubernatorov, M. Sannikov, I. Mikhailchuk, E. Kuznetsov, M. Artemov, O. F. Ouwatobi, M. Fernando, A. Asanov, Z. Guo, and D. Tsetserukou. Hapticvla: Contact-rich manipulation via vision-language-action model without inference-time tactile sensing. *arXiv preprint arXiv:2603.15257*, 2026.
- [36] C. Morissette, A. Abyaneh, W.-D. Chang, A. Houssaini, D. Meger, H.-C. Lin, J. Tremblay, and G. Dudek. Tactile modality fusion for vision-language-action models. *arXiv preprint arXiv:2603.14604*, 2026.
- [37] E. Perez, F. Strub, H. De Vries, V. Dumoulin, and A. Courville. Film: Visual reasoning with a general conditioning layer. In *Proceedings of the AAAI conference on artificial intelligence*, volume 32, 2018.
- [38] S. Liu, B. Li, K. Ma, L. Wu, H. Tan, X. Ouyang, H. Su, and J. Zhu. Rdt2: Exploring the scaling limit of umi data towards zero-shot cross-embodiment generalization. *arXiv preprint arXiv:2602.03310*, 2026.
- [39] C. Wang, H. Shi, W. Wang, R. Zhang, L. Fei-Fei, and C. K. Liu. Dexcap: Scalable and portable mocap data collection system for dexterous manipulation. *arXiv preprint arXiv:2403.07788*, 2024.
- [40] O. Siméoni, H. V. Vo, M. Seitzer, F. Baldassarre, M. Oquab, C. Jose, V. Khalidov, M. Szafraniec, S. Yi, M. Ramamonjisoa, et al. Dinov3. *arXiv preprint arXiv:2508.10104*, 2025.
- [41] J. Bi, K. Y. Ma, C. Hao, M. S. Zheng, and H. Soh. Vla-touch: Enhancing vision-language-action model with dual-level tactile feedback. *IEEE Robotics and Automation Letters*, 2026.
- [42] P. Hao, C. Zhang, D. Li, X. Cao, X. Hao, S. Cui, and S. Wang. Tla: Tactile-language-action model for contact-rich manipulation. *arXiv preprint arXiv:2503.08548*, 2025.
- [43] J. Li, T. Wu, J. Zhang, Z. Chen, H. Jin, M. Wu, Y. Shen, Y. Yang, and H. Dong. Adaptive visuo-tactile fusion with predictive force attention for dexterous manipulation. In *2025 IEEE/RSJ International Conference on Intelligent Robots and Systems (IROS)*, pages 3232–3239. IEEE, 2025.
- [44] S. Yu, K. Lin, A. Xiao, J. Duan, and H. Soh. Octopi: Object property reasoning with large tactile-language models. *arXiv preprint arXiv:2405.02794*, 2024.
- [45] C. Zhang, P. Hao, X. Cao, X. Hao, S. Cui, and S. Wang. Vtla: Vision-tactile-language-action model with preference learning for insertion manipulation. *arXiv preprint arXiv:2505.09577*, 2025.
- [46] J. Zhao, Y. Ma, L. Wang, and E. H. Adelson. Transferable tactile transformers for representation learning across diverse sensors and tasks. *arXiv preprint arXiv:2406.13640*, 2024.

- [47] H. Choi, J. E. Low, T. M. Huh, S. Hong, G. A. Uribe, K. A. Hoffmann, J. Di, T. G. Chen, A. A. Stanley, and M. R. Cutkosky. Coinft: A coin-sized, capacitive 6-axis force torque sensor for robotic applications. *arXiv preprint arXiv:2503.19225*, 2025.
- [48] S. Q. Liu and E. H. Adelson. Gelsight fin ray: Incorporating tactile sensing into a soft compliant robotic gripper. In *2022 IEEE 5th International Conference on Soft Robotics (RoboSoft)*, pages 925–931. IEEE, 2022.
- [49] J. Zhao and E. H. Adelson. Gelsight svelte: A human finger-shaped single-camera tactile robot finger with large sensing coverage and proprioceptive sensing. In *2023 IEEE/RSJ International Conference on Intelligent Robots and Systems (IROS)*, pages 8979–8984. IEEE, 2023.
- [50] S. Wang, Y. She, B. Romero, and E. Adelson. Gelsight wedge: Measuring high-resolution 3d contact geometry with a compact robot finger. In *2021 IEEE international conference on robotics and automation (ICRA)*, pages 6468–6475. IEEE, 2021.
- [51] W. K. Do and M. Kennedy. Densetact: Optical tactile sensor for dense shape reconstruction. In *2022 International Conference on Robotics and Automation (ICRA)*, pages 6188–6194. IEEE, 2022.
- [52] M. H. Tippur and E. H. Adelson. Gelsight360: An omnidirectional camera-based tactile sensor for dexterous robotic manipulation. In *2023 IEEE International Conference on Soft Robotics (RoboSoft)*, pages 1–8. IEEE, 2023.

A Task Definitions and Generalization Settings

In this section, we first propose the generalization settings and then describe the task progress definitions in detail.

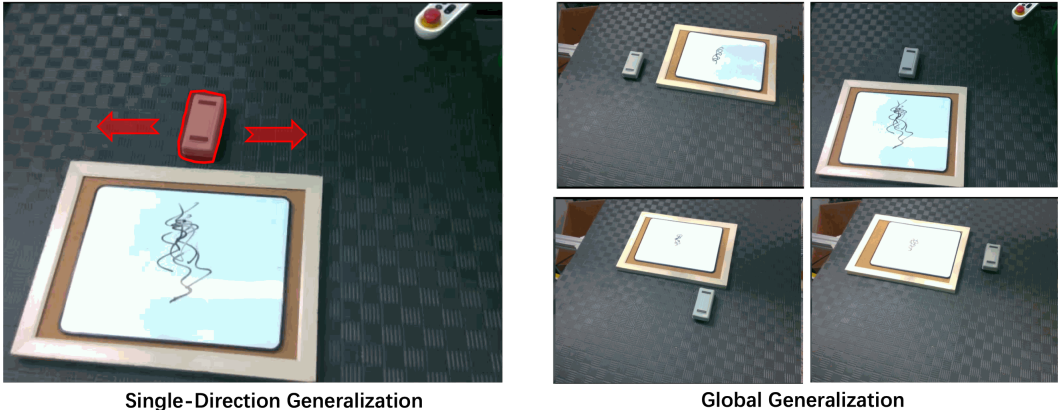


Figure 8: Generalization setting on our task. The left shows single-direction generalization, where only the eraser moves horizontally, and the vertical relative pose between the board and the eraser remains unchanged. The right shows global generalization, where the eraser and the board can have any relative relationship and location.

A.1 Generalization Setting

Vision-Language-Action (VLA) models exhibit certain generalization capabilities with large amounts of data, but remain challenging in limited-data scenarios. To this end, we first collect about 200 episodes of data to verify the data collection efficiency of our proposed AetheRock. In this setting, we collect data and infer within single-direction generalization to ensure task execution. Then, we collect 490 episodes of data to verify the post-training scaling law and vision-tactile learning across global generalization. The visualization is referred to in Figure 8.

A.2 Task Progress Definition.

In this subsection, we describe the definition of task progress in detail. We first include six tasks, Clamp Seal, Towel Hanging, Pick Bread, Erase Board, Pick Block, and Insert Flower, and collect about 200 episodes for each task. Then, we collect four tasks, Erase Board, Screwdriving, Close Bottle, and Stowing, and collect about 490 episodes for each task. The detailed task progress definitions can be found in Table 4.

B Details of GelSlim-MiniFab

In this section, we describe the manufacturing of the GelSlim-MiniFab in detail. Then, we provide visualizations of the GelSlim-MiniFab in contact with objects.

B.1 Manufacturing of GelSlim-MiniFab

Step 1: Mold Installation. To maximize gel consistency and provide a simple dismantling design to keep the gel complete and clean, we designed a shell to keep a consistent silicone thickness and protect useful components. Different parts are fixed with a hot-melt glue gun. After fixing, we isothermally cure the fixed shell for post-processing annealing, which ensures no bubbles form during subsequent heating of the printer material.

Task Name	Score	Description
Erase Board	0	Strike the desktop. Failed to pick up the eraser.
	0.1	Successfully grasped, it continued downward to strike the desktop.
	0.3	Successfully picked but resulted in contactless phantom erasing.
	0.7	Successfully picked, while partially erasing blackboard marks.
	1.0	Successfully picked and erased all blackboard marks.
Screw	0	Dislodged the socket. Impacted the socket.
	0.2	The socket was not picked up; instead, it was screwed while being pulled out.
	0.5	The socket was successfully picked up but misaligned; it was screwed while being pulled out.
	0.6	The socket was successfully picked up but not aligned with the screw; nonetheless, the screwing operation was successful. The socket was successfully picked up and aligned with the screw; consequently, it was screwed smoothly.
	0.8	The socket was successfully picked up and aligned with the screw; however, it was screwed while being pulled out or tilted.
	1.0	The socket was successfully picked up and aligned with the screw; consequently, it was screwed smoothly.
Close Bottle	0	Failed to pick up the lid.
	0.2	Successful pickup with the support block.
	0.3	Successfully picked up the lid, then moved and struck the bottle.
	0.4	Successfully picked up the lid, then moved above the bottle without aligning with the bottle opening.
	0.6	Successfully picked up the lid and aligned it with the bottle opening, but failed to lower it onto the bottle.
	0.8	Successfully picked up the lid and aligned it with the bottle opening, but it tilted during rotation.
	1.0	Successfully picked up the lid, aligned it with the bottle opening, and rotated it smoothly.
Stowing	0	Strike the block.
	0.1	Incorrect picking order.
	0.3	Successfully picked and placed the first block.
	0.6	Successfully picked and placed the first two blocks.
	1.0	Successfully picked and placed all blocks.

Table 4: Definition of Task Progress. Following $\pi_{0.5}$, we define task progress to evaluate policy performance in detail rather than relying solely on the success rate.

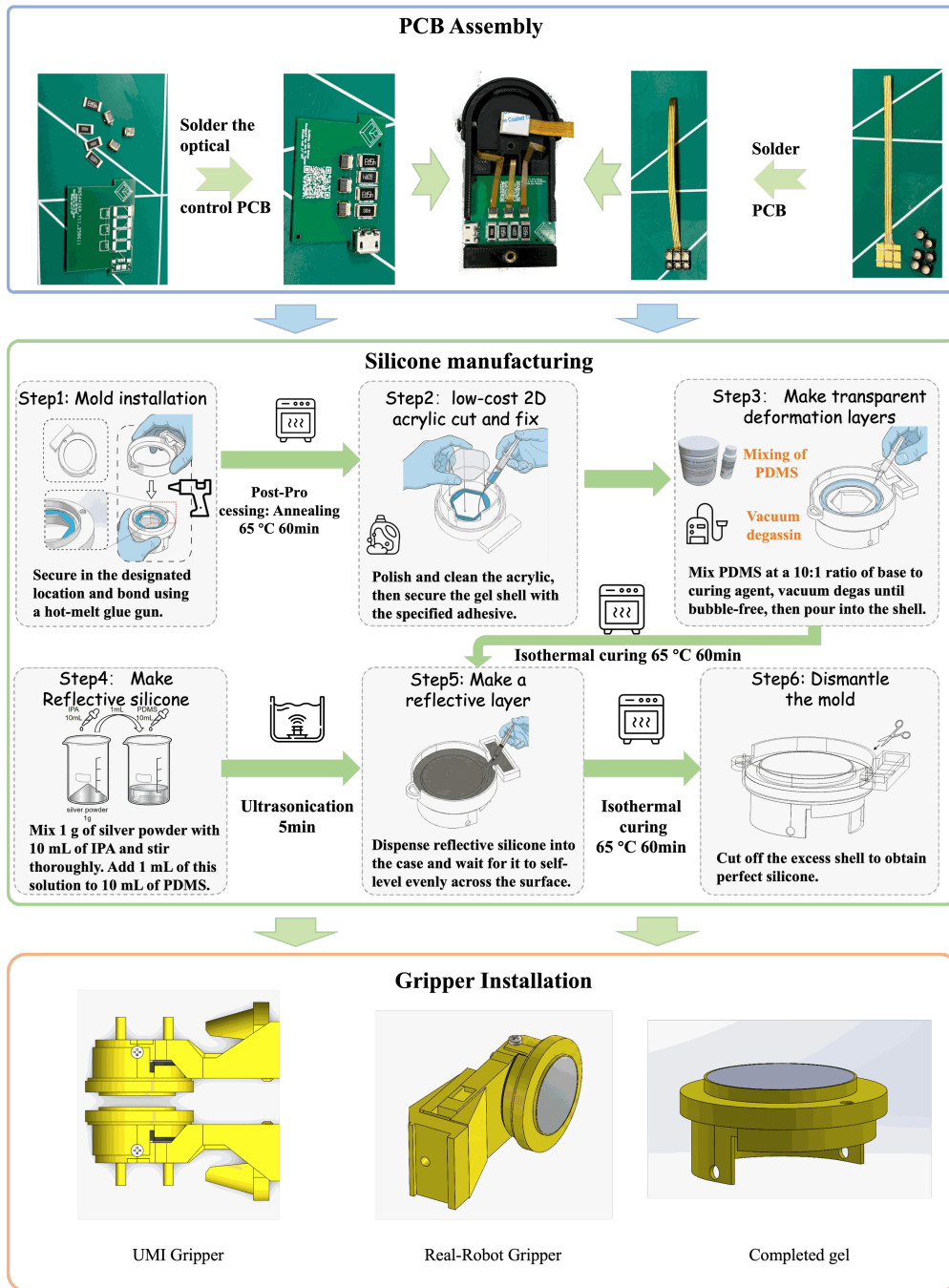


Figure 9: Detailed Manufacturing of GelSlim-MiniFab. Inspired by GelSlim 4.0 for the PCB assembly, we propose a silicone manufacturing method featuring low cost and easy repair. Finally, the completed gel is installed on the UMI and the real-robot device.

Step 2: Low-Cost 2D acrylic cut and fix. The translucent acrylic used in GelSlim 4.0 [17] has a 3D shape, and its manufacturing requires not only vertical cutting but also side grinding. The cost of manufacturing this is 10 times higher than simple vertical cutting. Alternatively, we refined the optical router to ensure it can adapt to only vertical cutting. To further ensure the acrylic surface is smooth, we used acrylic cleaning liquid to dissolve the edge burrs. Then, the smoothed acrylic is fixed to the gel shell using acrylic adhesive.

Step 3: Make transparent deformation layers. In this paper, we select PDMS as our gel material due to its advantages of good flexibility, low recovery latency, and high transparency. The base agent and curing agent are mixed at a 10:1 mass ratio. Based on the rapid curing feature of PDMS, and considering both the printer’s melting point and PDMS properties, we set the curing condition at 65 Celsius for 60 minutes.

Step 4: Make Reflective silicone. The reflective layer is used to exhibit contact deformation. If it is too thin, it will become translucent, whereas if it is too thick, it will decrease tactile precision. Through a large amount of empirical testing, we found that adding one gram of ultrafine silver powder to 10 ml of IPA, and then mixing 1 ml of this solution with PDMS yields the best results. Each mixing step utilizes ultrasonication to attain a consistent mixture. The mixed gel subsequently undergoes a vacuum operation to prevent any bubbles in the gel.

Step 5: Make a Reflective layer. After being heated, the transparent deformation layer is combined with reflective silicone to form a reflective layer. Specifically, the reflective silicone is poured into the groove and then flows out through the outlet. It is allowed to stand for 10 minutes to stabilize, and is then heated at a constant temperature of 65 degrees Celsius for 60 minutes.

Step 6: Dismantle the mold. Finally, we cut away the support material around the silicone and optionally stick it to the edge with glue to enhance stability.

B.2 Visualization of Dynamic Contact

Figure 10 shows the dynamic testing results of our proposed GelSlim-MiniFab sensor. The left column displays the standard objects used for tactile evaluation. Within each group, the top-right panel presents the calibrated raw tactile image, while the bottom-right panel displays the calibrated difference image relative to the no-contact reference. Overall, our visuo-tactile sensor demonstrates highly pronounced tactile perception. To fully preserve all tactile information—including contact geometry, tangential force, and other contact features—we utilize the calibrated tactile images directly as the model input.

C Experiment Setting and Results Analysis.

C.1 Detailed Training and Inference Setting

Training Setting. All policies used $\pi_{0.5}$ [4] as the pretrained model for post-training on the collected data. Aside from ForceVT, we used four NVIDIA H200 GPUs with a batch size of 128 to train the policy. The number of steps was set to 100,000 with a warmup cosine decay. The warmup steps were set to 1,000, and the peak learning rate was $2.5e-5$, the decay learning rate was $2.5e-6$, and the decay steps were 30,000. The training was conducted with the default AdamW optimizer with beta1 and beta2 set to 0.9 and 0.95, respectively. For ForceVT, the training data was split into seven groups: one from 75% and 50% fidelity tactile data, and five from 100% fidelity data. The batch size was set to 144 to maximally divide the data into each group.

Inference Setting. We implemented inference on a Flexiv Rizon 4 robot arm with a Flexiv Grav adaptive gripper. Figure 11 shows the installation of our visuo-tactile gripper on the Flexiv Grav adaptive gripper, which maintains a consistent structure as AetheRock. All policies used gripper

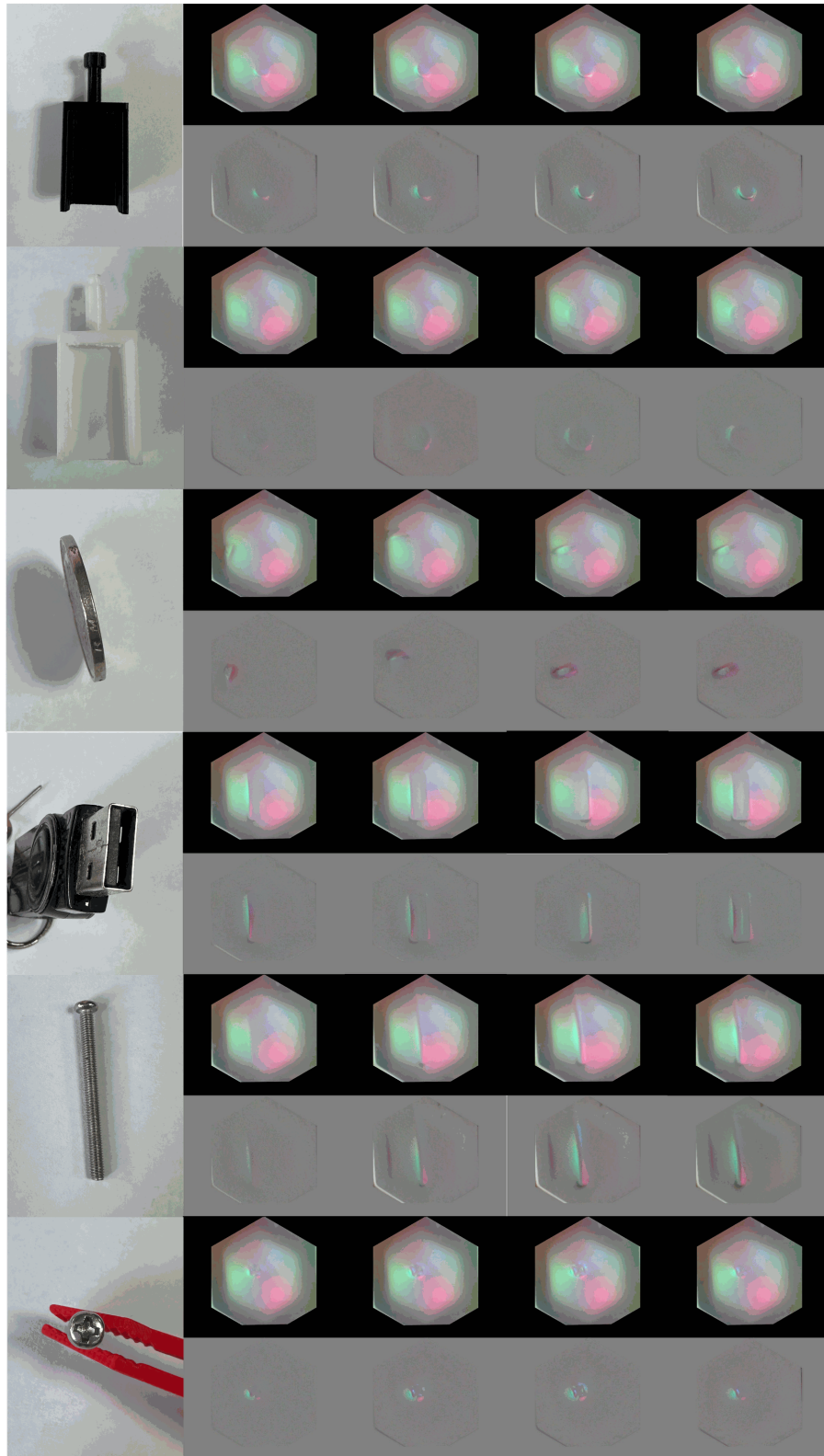


Figure 10: Visualization of dynamic contact for GelSlim-MiniFab. The left shows the object used to test the dynamic changes in tactile sensing. The top right of each group is the calibrated tactile image, and the bottom right is the relative difference computed between non-contact frames.

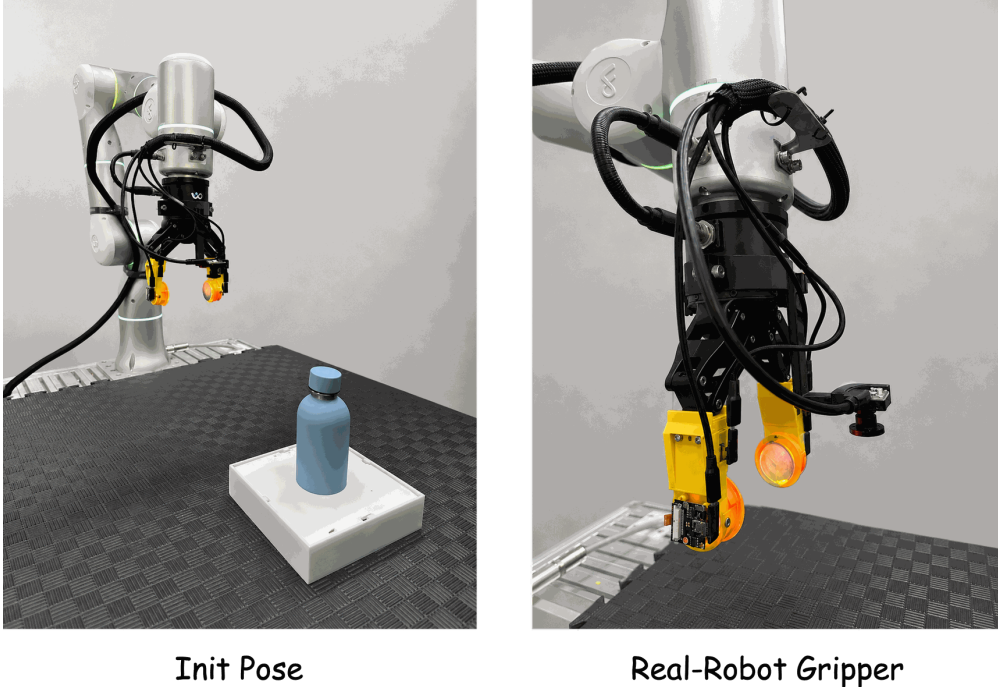


Figure 11: Real-robot inference setting. The left shows the initial pose during inference. Since the initial pose is sensitive for UMI-related inference, for a fair comparison, we select locations above and behind the default arm home pose as our general initial poses. The right shows the real-robot gripper, which maintains a consistent relative location between the end-effector and the camera.

width control rather than binarization. Since UMI is learned with relative poses, the init pose is important for inference. In our experiments, we used a unified init pose across all policies, which is higher and further behind than the Flexiv home pose, as shown in Figure 11. The robot control frequency was set to 10 Hz. The default $\pi_{0.5}$ model predicts a 50-step action, and the first 20 steps are input for the model to execute.

C.2 Detailed Result Analysis.

Figures 12 and 13 show the detailed results of the post-training scaling law and vision-tactile learning methods on four long-horizon tasks: board erasing, screwing, bottle closing, and stowing. Each figure includes a line chart of the average task progress, along with a heatmap reflecting the distribution of different scores across all inferences.

Figure 12 demonstrates that, overall, the average task progress consistently improves as the volume of data increases. However, distinct tendencies emerge across different tasks: board erasing and bottle closing exhibit more substantial improvements with data scaling. In contrast, stowing displays a different trend, where the marginal improvement diminishes in later data scaling stages. For the screwing task, additional data enables the model to thoroughly resolve edge-case errors. Furthermore, the heatmaps clearly illustrate that these macro-level improvements correspond to deeper progression within individual tasks. In tasks with a strong improvement trend, progress across all stages advances to varying degrees. Conversely, for stowing, which shows only slight improvement, the advancement is confined to a few inference cases shifting from low to high task progress.

Figure 13 shows the results of different visuo-tactile learning methods. Compared to the vision-only baseline, the simple visuo-tactile linear fusion method yields performance improvements in board erasing, bottle closing, and stowing. However, TacFilm and TactileConcat underperform relative to this simple linear fusion baseline. We speculate that two main reasons account for this

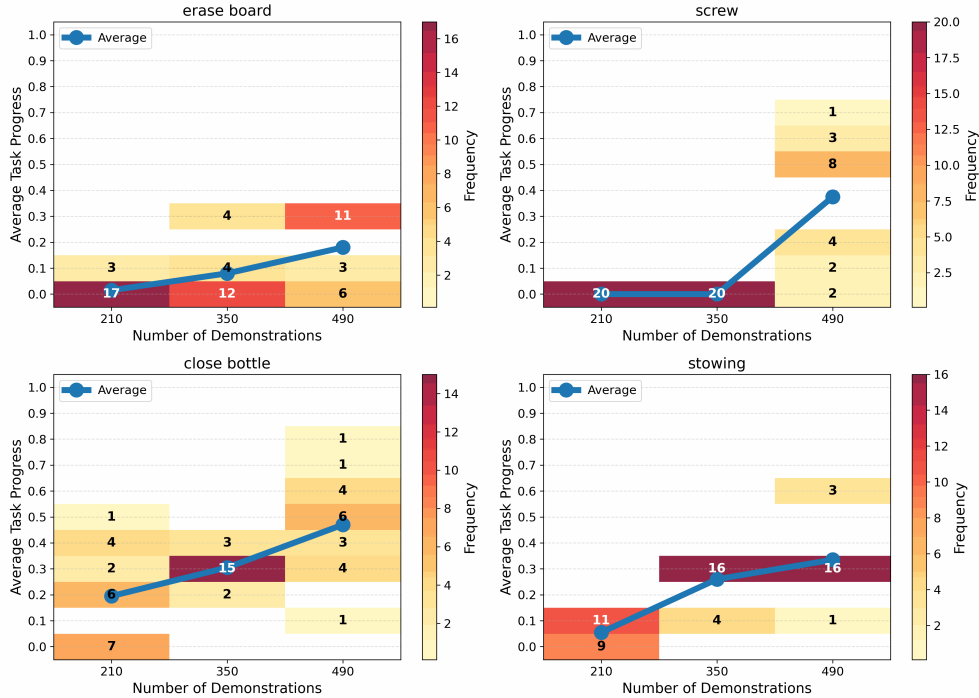


Figure 12: Results on the Post-Training Scaling Law. Each subfigure shows the results for one task. The lines show the average task progress using 210, 350, and 490 episodes of data, while the heatmaps indicate the distribution of scores across all evaluation runs.

Method	Average Task Progress (%)
VisTacLinear	47.0%
+ ForceVision-Tactile Softalign	52.0%
+ Cross-Modality Alignment	56.0%
+ Tactile Random Masking	58.0%

Table 5: Ablation study of different training strategies. Our method includes a simple visuo-tactile fusion module, Tactile Random Masking, Force-Vision-Tactile Soft Alignment, and a Cross-Modality Alignment core module. We iteratively ablate each module to evaluate its importance.

outcome. First, early fusion strategies underperform compared to late concatenation fusion when training data is limited during post-training. Second, the cross-sensor tactile representation exhibits poor generalization. Specifically, TactileConcat utilizes T3 [46] as its pretrained model, which was trained on datasets from GelSight Finray [48], GelSight Svelte [49], GelSight Wedge [50], DenseTact 2.0 [51], and GelSight 360 [52]. These sensors exhibit substantial discrepancies compared to our proposed GelSlim-MiniFab. As described in the main paper, in the screwing task, out-of-distribution (OOD) tactile inference severely degrades performance, leading to lower metrics than the vision-only baseline. In contrast, by incorporating force information and achieving better alignment across all modalities, our ForceVT consistently improves performance across all tasks.

C.3 Ablation Study

Table 5 shows the ablation results for our proposed ForceVT method. Overall, the full ForceVT framework comprises several core components: simple vision-tactile linear fusion, Tactile Random Masking (following DINOv3 [40]), soft force-vision-tactile alignment, and cross-modality alignment. The results indicate that both the force-vision-tactile alignment and cross-modality alignment yield relatively larger improvements compared to tactile random masking. However, when consider-

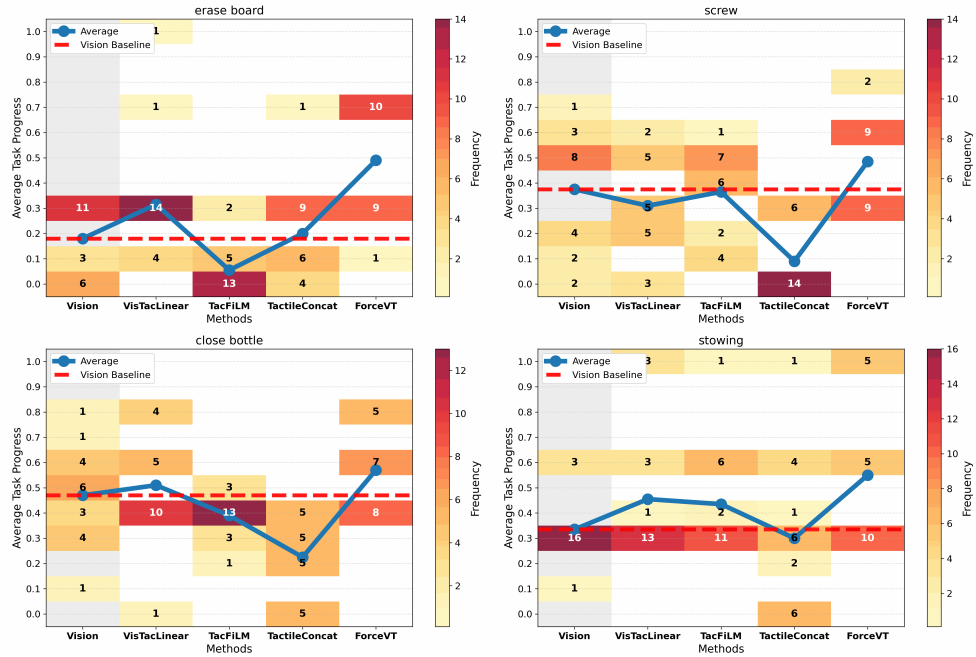


Figure 13: Results of different vision-tactile learning algorithms. Each subfigure indicates the results for one task. The lines indicate the average task progress, and the heatmaps indicate the distribution of scores across all inference experiments. The dark background highlights the results without tactile input, whereas all other methods include tactile input. The red line shows the vision-only results.

ing the robustness results presented in the main paper, tactile random masking significantly enhances inference robustness across various challenging tactile conditions.